

# Site correlation effects in the dynamics of iron impurities $\text{Fe}^{2+}/\text{Fe}^{3+}$ and antisite defects $\text{Nb}_{\text{Li}}^{4+}/\text{Nb}_{\text{Li}}^{5+}$ after a short-pulse excitation in $\text{LiNbO}_3$

J. Carnicero,<sup>1</sup> M. Carrascosa,<sup>1</sup> G. García,<sup>2</sup> and F. Agulló-López<sup>1,2</sup>

<sup>1</sup>Departamento de Física de Materiales C-IV, Universidad Autónoma de Madrid, 28049 Madrid, Spain

<sup>2</sup>Centro de Microanálisis de Materiales (CMAM), Universidad Autónoma de Madrid, 28049 Madrid, Spain

(Received 15 March 2005; published 12 December 2005)

The correlation effects between excitation and trapping sites after light excitation in a Li-deficient Fe-doped  $\text{LiNbO}_3$  crystal have been quantitatively analyzed. They appear as a direct consequence of the thermally activated random transport (hopping) of electrons (free polarons) by using a Monte Carlo approach. The physical consequences of those effects, not present in usual coherent band-transport analyses, are explored and discussed in the light of available experiment. In particular, nonexponential decay kinetics for the evolution of electrons trapped at antisites (small polarons) are predicted.

DOI: 10.1103/PhysRevB.72.245108

PACS number(s): 42.70.Nq, 42.70.Ln, 78.20.Bh

## I. INTRODUCTION

$\text{LiNbO}_3$  is a reference material for electrooptic and non-linear optical applications.<sup>1</sup> It is usually grown in the Li-deficient congruent composition ( $[\text{Li}]/[\text{Nb}]=0.945$ ) and so it is strongly defective. Two main models<sup>2-4</sup> have been proposed for the defects associated to the deviation from stoichiometry. One assumes that those intrinsic defects are Nb vacancies and  $\text{Nb}_{\text{Li}}$  antisites<sup>4</sup> (with a concentration around 4.8%). The other model supported by recent evidences, considers Li vacancies and also  $\text{Nb}_{\text{Li}}$  antisites<sup>2,3</sup> (in this case the  $\text{Nb}_{\text{Li}}$  concentration would be 1%). They show<sup>5,6</sup> a characteristic broad absorption band in the IR peaked at about 1.6 eV (780 nm). On the other hand iron-doped crystals show absorption and photoconductivity in the visible and near UV range. In fact, two valence states of iron  $\text{Fe}^{2+}$  and  $\text{Fe}^{3+}$  are well-known donors and traps, respectively, for free electrons. The donor state  $\text{Fe}^{2+}$  presents<sup>1,7</sup> a broad absorption band at  $\sim 500$  nm.

Most photoconductive (PC) and photorefractive (PR) experiments performed in congruent  $\text{LiNbO}_3$  crystals have been satisfactorily explained in terms of an one-center or two-center band-transport models.<sup>8-10</sup> The latter (more realistic) model involves light excitation of  $\text{Fe}^{2+}$  centers coherent motion through the conduction band, temporary trapping at  $\text{Nb}_{\text{Li}}^{5+}$  antisites, and final trapping at  $\text{Fe}^{3+}$  acceptor centers. In either of the two above models, coherent band transport is usually assumed. However, there is abundant experimental evidence that carrier transport occur via thermally activated random motion (hopping) of self-trapped electrons (free polarons).<sup>11-13</sup> Therefore, the models should be reformulated within this hopping-transport framework. Fortunately, CW experiments do not distinguish between the two transport mechanisms as it was early demonstrated in a detailed work by Feinberg *et al.*<sup>14</sup> The situation is different for short-pulse experiment. They are much more sensitive to the subtle details of the electron dynamics and to the interplay between the excitation and trapping centers. In particular, some spatial correlation between the excitation and the antisite trapping sites is expected that may significantly influence the after-pulse kinetics.

The purpose of this work is to discuss the correlation effects between excitation and trapping sites that cannot be properly handled in a band-transport model. They appear as a direct consequence of randomness in the hopping motion of electrons. In fact, the physical consequences of randomness in hopping transport models have been recently put forward in a very broad perspective by Sturman *et al.*<sup>15</sup> In our work, a Monte Carlo simulation approach has been developed to reach quantitative predictions for  $\text{LiNbO}_3$ . The physical consequences of these effects on the after-pulse kinetics are explored. It has been concluded that significant effects should be observed, such as a clear departure from the exponential kinetics derived from band-transport models when saturation is avoided. Therefore, spatial correlations may play a role in interpreting available experiments and should add or compete with other mechanisms previously invoked. The analysis could be readily extended to other materials where hopping transport has also been demonstrated.

## II. ELECTRON EXCITATION AND TRAPPING IN $\text{LiNbO}_3$ : HOPPING TRANSPORT

We will assume throughout the paper that free electrons in  $\text{LiNbO}_3$  self-trap at host Nb atoms and form free polarons.<sup>13,16</sup> They experience thermally activated random jumps between neighbor regular  $\text{Nb}_{\text{Nb}}$  ions.<sup>11,17</sup> The overall process proceeds as illustrated in the level scheme of Fig. 1. First we assume, in accordance with previous views, that illumination at the  $\text{Fe}^{2+}$  absorption band (2.60 eV) transfers<sup>7,12</sup> the excited

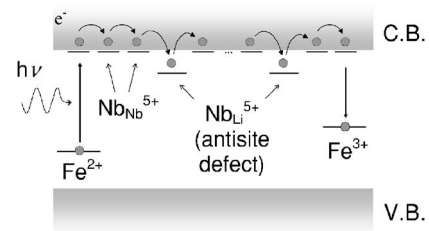


FIG. 1. Schematics of the light induced electron excitation, random walk across the lattice, and final retrapping.

electron to the nearest  $\text{Nb}^{+5}$  neighbors (charge transfer band). The position of the  $\text{Fe}^{+2}$  excited levels within the band gap has been obtained from  $X_\alpha$  calculations<sup>18,19</sup> although it is still a matter of controversy. The photoexcited electrons move, then, by random hopping through the host Nb lattice (diffusion like transport). The final fate of the electrons is being trapped at the  $\text{Fe}^{+3}$  acceptors, which are substitutionally located (as the  $\text{Fe}^{+2}$  donors) at the Li sites.<sup>20,21</sup> During the random motion and before recombining with the  $\text{Fe}^{+3}$  acceptors, they can be temporarily trapped at the more abundant  $\text{Nb}_{\text{Li}}^{+5}$  antisites forming small polarons. They are thermally unstable with a relatively long lifetime and decay in the dark so that the photogenerated electrons are transferred back to the iron centers. In the rest of the paper we will use the term polaron to refer to the small polarons.

The electron motion through the Nb sublattice is governed by the jump frequency  $\Gamma$  between regular nearest-neighbors atoms. The possibility of a tunneling contribution is here ignored although it cannot be ruled out. The jump frequency can be estimated from the measured diffusion coefficient for free polarons at room temperature (i.e., from the electron mobility). The values in the literature<sup>11,22,23</sup> are quite disperse covering the range  $D \approx 10^{-3} - 10^{-5} \text{ cm}^2 \text{ s}^{-1}$ . This leads to  $\Gamma \sim 10^{11} - 10^{12} \text{ s}^{-1}$ . We will take  $\Gamma = 10^{11} \text{ s}^{-1}$ , although it has been checked that all results presented in the paper are essentially independent of this particular choice. On the other hand, during the migration process the free electrons can be trapped by  $\text{Nb}_{\text{Li}}$  antisites or  $\text{Fe}^{+3}$  iron acceptors, which are both located in the Li sublattice. The corresponding trapping coefficients, as used in the band-transport model, are given by  $S_{\text{Fe}} = \Gamma V_{\text{Fe}}$  and  $S_A = \Gamma V_A$ ,  $V_A$  and  $V_{\text{Fe}}$  being the capture volumes of an antisite and an iron acceptor, respectively. They are expected to be of the order of the lattice volume per atom ( $V \sim 10^{-21} \text{ cm}^3$ ) so we will assume that they includes all host Li atoms that are nearest neighbors to the visited Nb atom. Therefore, one predicts,  $S_{\text{Fe}} = S_{\text{Nb}} = 10^{-10} \text{ cm}^3 \text{ s}^{-1}$ , which are comparable to the values used in band-transport models.

The electron trapped at the iron acceptor, i.e., the  $\text{Fe}^{+2}$  donor, is stable in the dark. On the other hand, the thermal stability of a filled antisite is described by a lifetime  $\Gamma_A^{-1}$  before jumping into a neighbor  $\text{Nb}_{\text{Nb}}$  ion. From some decay data,<sup>24</sup> this lifetime can be estimated around 1–10  $\mu\text{s}$ . We will take it to be 1  $\mu\text{s}$ . As to the photoionization cross section, the available information indicates that the ionization cross sections for  $\text{Fe}^{2+}(\sigma_{\text{Fe}})$  and  $\text{Nb}_{\text{Li}}^{4+}(\sigma_A)$  are of the same order of magnitude<sup>25,26</sup> for green light used in relevant experiments in the range  $1 - 8 \times 10^{-18} \text{ cm}^2$  at the peak of the corresponding absorption band. For convenience, we will take  $\sigma_{\text{Fe}} = \sigma_A = 5 \times 10^{-18} \text{ cm}^2$ .

### III. RANDOM WALK OF ELECTRONS: MONTE CARLO SIMULATIONS

#### A. Crystal structure

The simulation of electron transport requires an adequate knowledge of the crystal structure in  $\text{LiNbO}_3$ . The Nb and Li lie on rhombohedral sublattices having trigonal symmetry around the  $c$  axis, as illustrated in Fig. 2. They are identical

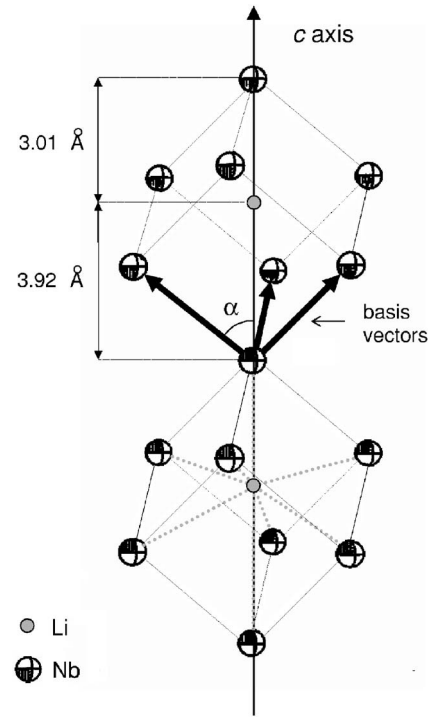


FIG. 2. Schematics of the Li and Nb sublattices of  $\text{LiNbO}_3$ .

except for a shift of 3.01  $\text{\AA}$  along that axis.<sup>27</sup> The three basic vectors of the primitive cell have a modulus of 3.76  $\text{\AA}$  and form an angle  $\alpha = 52.1^\circ$  with the  $c$  axis. It can be readily checked that the lattice is very close to cubic. Any Nb or Li lattice point can be labeled in that primitive basis by the generic coordinates  $(m, n, p)_{\text{Nb}}$  and  $(m, n, p)_{\text{Li}}$ , respectively. Each Nb (or Li) atom has six nearest Nb (or Li) neighbors at a distance of 3.76  $\text{\AA}$ . All other Nb (or Li) atoms are at further distances. On the other hand, each Li (or Nb) atom is at 3.05  $\text{\AA}$  from three Nb (or Li) neighbors contained in a plane perpendicular to the  $c$  axis, at 3.38  $\text{\AA}$  from another 3 Nb (or Li) atoms in a plane parallel to the previous one, and has two additional neighbors along the  $c$  axis at 3.01 and 3.92  $\text{\AA}$  (see Fig. 2 and Ref. 27). Li atoms can be occupied by a  $\text{Nb}_{\text{Li}}$  antisite or an Fe atom. In order to simplify the mathematical artillery, we will consider all these eight neighbor atoms equivalent from the point of view of electron transfer from a  $\text{Nb}_{\text{Li}}$  antisite defect.

#### B. Random walk of electrons

As previously mentioned, the migration and trapping of the photoexcited electrons will be simulated using a random-walk approach implemented with a Monte Carlo code. At the start of each history the electron will be excited from a generic  $\text{Fe}^{+2}$  atom, assumed to be located at  $(0, 0, 0)_{\text{Li}}$ . The excitation takes place at a random instant within the pulse duration generated according to an exponential law with constant  $\Gamma_{\text{Fe}}(I) = \gamma_{\text{Fe}} I$ , where  $\gamma_{\text{Fe}} = \sigma_{\text{Fe}} / h\nu$ . Photon absorption transfers the electron to the nearest neighbor Nb at  $(0, 0, 0)_{\text{Nb}}$  which is taken as the starting point of the migration process. From each  $(n, m, p)_{\text{Nb}}$  site the electron Random Walk of electrons jumps into one of the six nearest Nb neighbors that

occupy the sites  $(n \pm 1, m, p)_{\text{Nb}}$ ,  $(n, m \pm 1, p)_{\text{Nb}}$ , and  $(n, m, p \pm 1)_{\text{Nb}}$ , assuming equal probability for all jumps. The coordinates of the visited sites are properly stored along each history. At each visit to a  $\text{Nb}_{\text{Nb}}$  atom (not previously visited) the code decides whether there is a trap (either  $\text{Fe}^{+3}$  or  $\text{Nb}_{\text{Li}}^{5+}$ ) available in a nearest-neighbor location at the Li sublattice. If this is so, the electron is trapped. The decision is based on a random spatial distribution of the traps. Possible trapping at the original  $(0, 0, 0)_{\text{Li}}$  donor site is taken into account.

After the trapping, the next step depends on whether the time  $t < \tau$  or  $t > \tau$ . In the first case, we are still within the pulse duration and so one has to consider the light-induced ionization for the corresponding center  $\text{Nb}_{\text{Li}}^{4+}$  or  $\text{Fe}^{+2}$ . The lifetime for the  $\text{Nb}_{\text{Li}}^{4+}$  should include the thermal as well as the light-induced lifetime, i.e.,  $\Gamma_A(I) = \Gamma_A(0) + \gamma_A I$ , where  $\gamma_A = \sigma_A / h\nu$ . In other words, the electron will be kept at this position during a random time consistent with its lifetime  $\Gamma_A^{-1}(I)$ . The same scheme is followed for the  $\text{Fe}^{+2}$ , but considering only photoexcitation, with a lifetime  $\Gamma_{\text{Fe}}^{-1}(I)$ . In the other case, when  $t > \tau$  (the illumination is over) the  $\text{Fe}^{+2}$  center is completely stable and the corresponding history is finished. On the other hand, the lifetime for the  $\text{Nb}_{\text{Li}}^{4+}$  will be that one exclusively associated to thermal ionization  $\Gamma_A^{-1}(0)$ . The random-walk migration proceeds until the electron is finally trapped at an iron acceptor. This is the end of the corresponding history. The calculations typically include around  $10^5$  histories. The final information obtained from the simulated experiment include electrons that have been re-trapped at the initial iron center, location of the occupied antisites just after the pulse, and concentration of small polarons surviving at any time  $t$ .

#### IV. RESULTS OF MONTE CARLO SIMULATIONS

The results derived from the simulation program will be presented in two main steps. First, the total concentration of filled antisites at the end of the light pulse and its spatial distribution around the initial donor  $\text{Fe}^{+2}$  center will be given, as well as its dependence on light intensity and antisite concentration. These data will illustrate the site-correlation effects appearing in the process. Then, the overall kinetics of small polarons and iron centers will be given for several intensities. Data will refer to two relevant antisite concentrations corresponding to the values expected from the two main structural models for a congruent crystal: lithium vacancy model (1% antisites) and niobium vacancy model (4.8 % antisites).

##### A. Spatial correlation between excitation ( $\text{Fe}^{2+}$ ) and trapping ( $\text{Nb}^{4+}$ ) sites

This is a key information provided by our hopping model that cannot be provided by the standard band-transport approach. Let us look at the spatial (radial) distribution of the filled antisites just after the light pulse, but letting all surviving electrons become trapped at either iron or antisite centers. Simulation results for antisite concentrations of 1 and 4.8 % are, respectively, displayed in Figs. 3(a) and 3(b). The

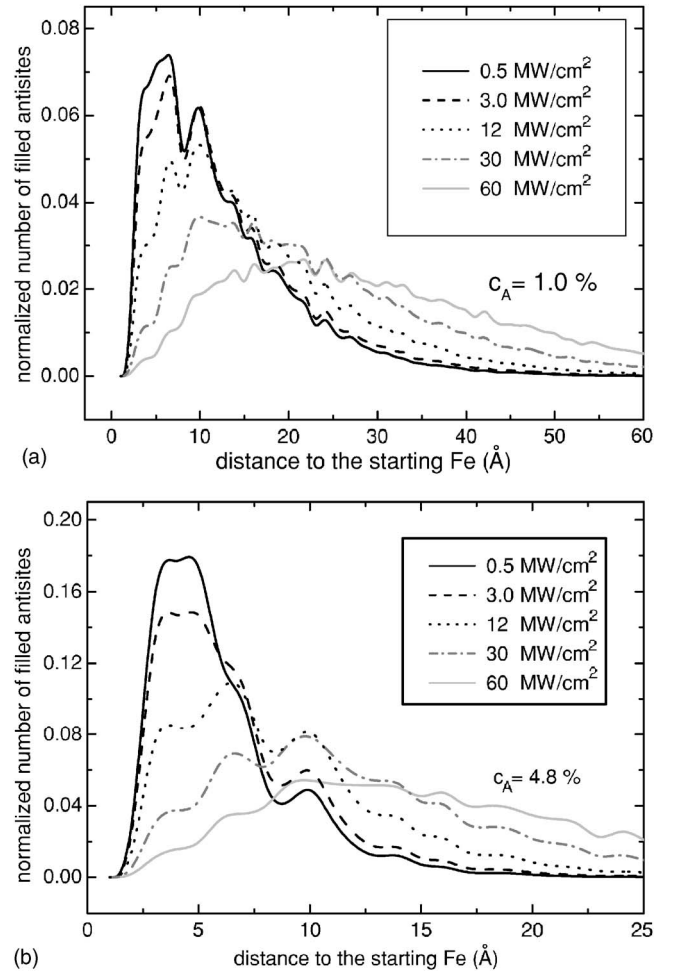


FIG. 3. Normalized distribution of filled antisites as a function of the distance from the origin to the first antisite visited after the end of the light pulse. Different light intensities are considered.

iron concentration has been fixed at the typical value of 1000 ppm, so the average distance between Fe traps is around 38 Å. The simulation results clearly illustrate the site correlation between the iron donor and the generated small polarons. In all cases the distribution is peaked at a short distance of the photoexcited iron donor, whereas beyond the peak region the distribution approaches an exponential decay. On the other hand, the correlation effects are progressively reduced on going to higher light intensities. This can be intuitively understood since higher intensities cause multiple excitations during the duration of the pulse, contributing to separate the photoexcited electron from its initial position.

The distributions corresponding to several antisite concentrations up to a maximum of 5% (roughly corresponding to a niobium vacancy model in a congruent crystal) are depicted in Fig. 4. Data for two light intensities, one in the linear response region [1 MW/cm<sup>2</sup>, Fig. 4(a)] and the other in the saturation stage [40 MW/cm<sup>2</sup>, Fig. 4(b)] are shown. Iron concentration is again 1000 ppm. The simulation results show the progressive smearing out of the site-correlated distribution on moving to smaller antisite concentrations. In fact, the position of the distribution peak shifts to longer distances and its height decreases when the antisite concen-

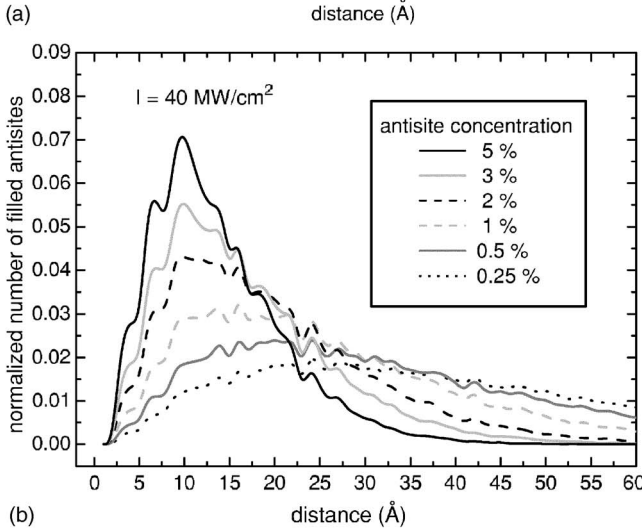
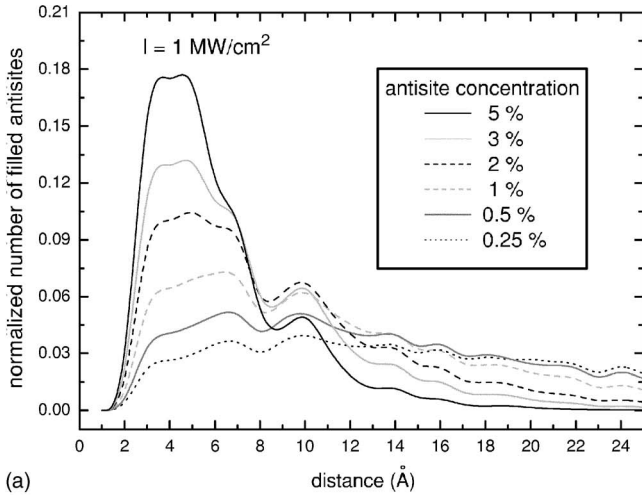


FIG. 4. Normalized distribution of filled antisites as a function of the distance from the origin to the first antisite visited after the end of the light pulse. Different antisite concentrations are considered.

tration is reduced. Moreover, the peak becomes progressively broader. Figure 5 shows the dependence of the position of the maximum of the distribution and its height as a function of the antisite concentration for the two investigated light intensities. In conclusion, correlation effects progressively disappear for increasing crystal stoichiometry. For the usual antisite concentrations and iron-doping levels most electrons have been trapped in the near vicinity of the photoexcited iron, where the presence of other iron ions is hardly probable.

**B. Limit case of a  $\delta$ -type pulse: Analytical approach**

It is interesting for comparison purposes to plot the radial distribution of the electrons trapped at an antisite following a  $\delta$ -type light pulse. This is a limit case that should approximately reproduce the data obtained for a sufficiently short pulse and arbitrary light intensities. One interesting feature of the  $\delta$  case is that the trapped electron distribution can be well approximated by the following analytical expression

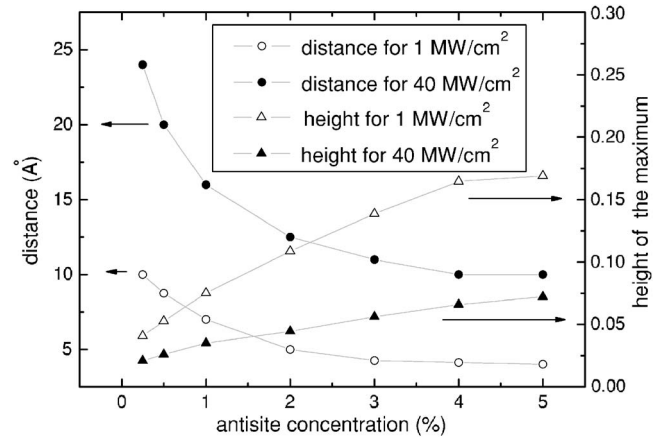


FIG. 5. Position and height of the peak value in the radial frequency distribution as a function of antisite concentration for two values of light intensity.

which strictly applies for a cubic lattice, in which retrapping at the origin is neglected:

$$f(R) = 4\pi R^2 \sum_{N=1}^{\infty} \frac{ae^{-a(N-1)}e^{-R^2/(2N/3)}}{(2\pi N/3)^{3/2}}, \quad (1)$$

where  $R$  is the distance to the origin measured in lattice constant units,  $N$  is the number of steps, and  $a$  a constant whose meaning is explained below. Figure 6 shows the comparison of this analytical formula and the Monte Carlo results for a delta-type light pulse. A reasonable agreement is observed.

The physical arguments behind such expression are as follows: one may assume that the probability  $p(N)$  of being trapped at step  $N+1$ , after  $N$  steps, where trapping has not occurred, is a quantity  $a$ , independent of the step number  $N$ . The value of this constant can be expressed as  $a=c\frac{5}{6}f$ , where  $c$  is the antisite concentration. The factor  $5/6$  takes into ac-

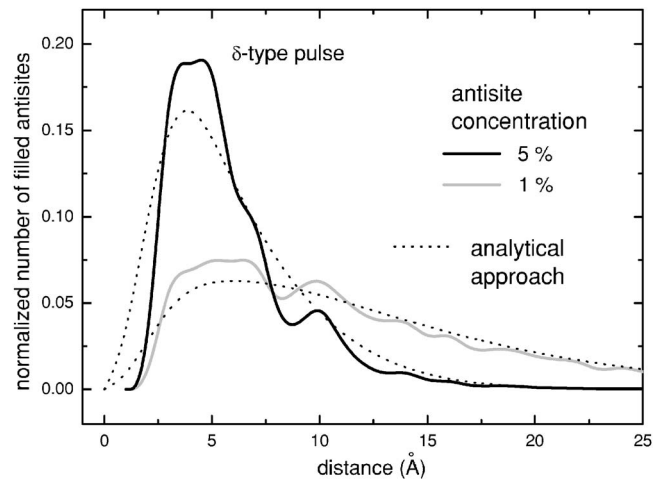


FIG. 6. Normalized distribution of filled antisites as a function of the distance from the origin to the first antisite visited after a  $\delta$ -type light pulse. An analytical approach, given by Eq. (1), is also depicted for the two chosen antisite concentrations.

count the fact that one of the six nearest neighbors has been visited in the previous step, and  $f$  assumes the probability that some other nearest neighbors has been visited before. The value of  $f$  can be derived from direct comparison to the Monte Carlo results, yielding  $f \approx 0.912$ . This implies that the probability distribution for the random variable  $N$  is approximately exponential  $p(N) = ae^{-a(N-1)}$ .

Once this behavior  $p(N)$  is known, it is very simple to apply the well-known result of random walk theory about the radial distribution of the presence probability per unit volume after a fixed number of steps  $N$ . This probability can be expressed as  $p(R|N) = f(R) dx dy dz$ , where  $f(R)$  follows Gaussian statistics with sigma equal to  $\sqrt{N/N_d}$ ,  $N_d$  being the dimensionality of the problem ( $N_d = 3$  in our case). Therefore we have

$$p(R|N) = \frac{e^{-R^2/(2N/3)}}{(2\pi N/3)^{3/2}} dx dy dz = 4\pi R^2 \frac{e^{-R^2/(2N/3)}}{(2\pi N/3)^{3/2}} dR. \quad (2)$$

Finally, the probability density function  $p(R)$  that we want to obtain can be readily calculated by conditioning its distribution to the random variable  $N$  and integrating over its full range of definition, namely,  $p(R) = \sum_{N=1}^{\infty} p(R|N)p(N)$  which yields the final proposed expression (1).

## V. PHYSICAL EFFECTS CAUSED BY THE SITE CORRELATION

Now we will discuss the physical effects caused by the above site correlation effects (SCE). At a qualitative level, they are in line with experimental data recently observed and should be considered in future rigorous treatment of the after-pulse kinetics.<sup>24,28</sup>

### A. Intensity dependence and saturation effects

The dependence of the total concentration of electrons trapped at  $\text{Nb}_{\text{Li}}^{+5}$  antisites on light intensity is shown in Fig. 7. It covers the intensity range from 1 to 60  $\text{MW}/\text{cm}^2$ . Two antisite concentrations have been used in the simulations: 1% (Li vacancy model for a congruent crystal) and 4.8% (Nb vacancy model for a congruent crystal). The data points show a linear dependence at low intensities but start to deviate from it for  $I \geq 5 \text{ MW}/\text{cm}^2$  (saturation effects), in qualitative accordance with experimental data obtained in Refs. 24 and 28. On the other hand, the relative concentration of  $\text{Fe}^{2+}$  donors that remain occupied at the end of the pulse is the complementary (with regard to 1) of the values for the antisite concentrations plotted in Fig. 7. The curves ignoring SCE (i.e., ignoring the position of the original excited  $\text{Fe}^{2+}$  for each electron history) have also been plotted for comparison. It can be seen that when ignoring SCE, the curves saturate at lower intensities and the absorption bands are higher. This effect can be explained as follows: when the possibility of electron trapping at the original Fe center is enabled, the relative probability for trapping at a  $\text{Nb}_{\text{Li}}$  center increases. Finally, it can be expected that the hopping model results neglecting SCE are equivalent to the band transport model predictions. This has been checked solving the band transport equations as presented in Ref. 10 with the same material

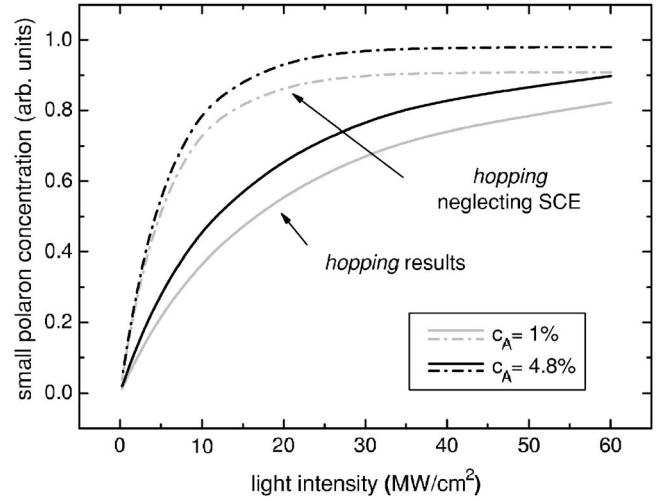


FIG. 7. Small polaron concentration reached just after a 10 ns pulse as a function of light intensity. The *hopping* neglecting SCE predictions (dash-dotted line) has been also included for comparison.

parameters and experimental conditions simulated in Fig. 7. As expected, the obtained curves exactly coincide with the hopping model neglecting SCE.

### B. After-pulse kinetics in the dark

The objective of this section is to find out how SCE influences the overall kinetics of the process. After the light pulse (i.e., in the dark), the small polarons decay thermally and electrons go back to the iron acceptors. Although the average distributions of filled antisites and iron centers are uniform along the crystal, a fraction of the antisites have a correlated close-by iron corresponding to the original donor, as illustrated in the previous section. The time evolution in the dark of the polaron concentration is represented in Fig. 8 for several light pulse intensities. The concentration is given

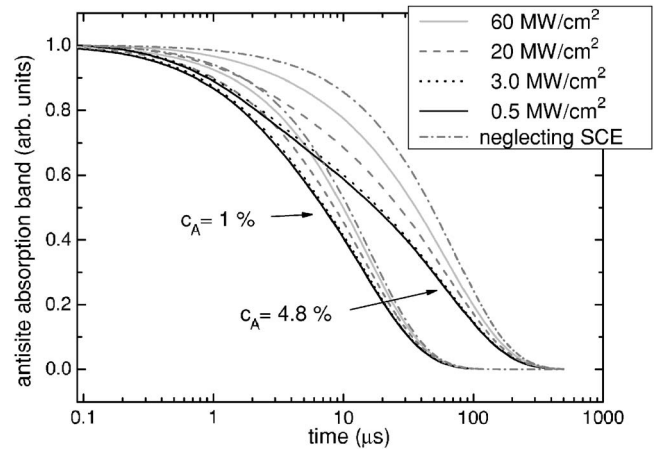


FIG. 8. Time evolution of the antisite absorption band intensity normalized to its initial value for different pumping light intensities and antisite concentrations, as given by the Monte Carlo model. The hopping neglecting SCE predictions (dash-dotted line) has been also included for comparison.

in a linear scale whereas time is plotted in a log scale. For comparison, the polaron decays predicted by the hopping model ignoring SCE are also shown in the figure. As in the previous section (A), it has been checked that these latter curves coincide with the BT predictions. It is clear that in the hopping model the decay deviates from an exponential law, as experimentally observed by Berben *et al.*<sup>24</sup> The deviation is larger for the lower intensities as expected from the larger site-correlation effects (see Fig. 3). The faster decay obtained when SCE effects are present is easy to understand. At the end of the pulse, an important amount of excited electrons have formed small polarons in the vicinity of the “original” Fe center (see Fig. 3). Therefore, they have a relatively high probability to be trapped at this center during subsequent migration in the dark. This fraction of electrons become trapped within an average time much smaller than electrons trapped at Fe<sup>+3</sup> placed at random position from the “original” Fe center. The shape of the decay curves has been analyzed using either a single exponential, a two-exponential, and a stretched exponential law  $n=n(0)\exp\{-(t/\tau)^\beta\}$ . The fitting appears reasonable in the two latter cases, as illustrated in Fig. 9. One should remark that the difference between a two-exponential and a stretched exponential relaxation is not often obvious and the example of polymer relaxation is illustrative.<sup>29</sup>

## VI. SUMMARY AND CONCLUSIONS

A theoretical model has been developed to describe the kinetics of iron and niobium antisite centers, during and after a short light excitation pulse of green light. It is based on hopping electron transport and is alternative to standard two-center approaches assuming coherent band transport. A Monte Carlo code has been used to simulate the electron dynamics. The key feature of the hopping model is the strong spatial correlation between donor and acceptor sites that accounts for significant deviations from the predictions of band transport approaches. The SCE are a direct consequence of

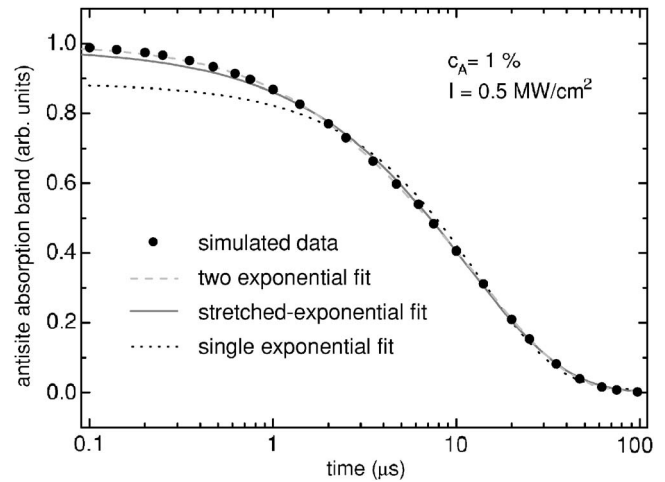


FIG. 9. Monte Carlo results for the normalized time evolution of the antisite absorption band intensity for a chosen value of  $I = 0.5 \text{ MW/cm}^2$  and  $c_A = 1\%$ , fitted to several functions. The time constants for these functions are: single exponential fitting  $\tau = 13.3 \mu\text{s}$ , double-exponential fitting  $\tau_1 = 2.38 \mu\text{s}$  and  $\tau_2 = 15.56 \mu\text{s}$ , and stretched-exponential fitting  $\tau = 11.48 \mu\text{s}$  and  $\beta = 0.812$ .

the random motion of electrons in the LiNbO<sub>3</sub> lattice. Other models explain these site-correlation effects in terms of a direct electron transfer between iron and niobium antisite centers, which is introduced in a phenomenological way. Additional experiments should be performed to clarify the contribution of each of these approaches to the observed kinetic behavior.

## ACKNOWLEDGMENTS

We want to thank Professor José Manuel Cabrera for useful discussions and comments. This work was supported by the Spanish Ministerio de Educación y Cultura under Grant No. MAT2002-03220 and the Comunidad de Madrid (Project No. GR/MAT/0514/2004).

<sup>1</sup> *Properties of Lithium Niobate*, edited by K. K. Wong, EMIS Datareview Series No. 28 (INSPEC, IEE, London, 2002).

<sup>2</sup> J. Blümel, E. Born, and Th. Metzger, *J. Phys. Chem. Solids* **55**, 589 (1994).

<sup>3</sup> F. P. Safaryan, R. S. Feigelson, and A. M. Petrosyan, *J. Appl. Phys.* **85**, 8079 (1999).

<sup>4</sup> B. C. Abrahams and P. Marsh, *Acta Crystallogr., Sect. B: Struct. Sci.* **42**, 61 (1986).

<sup>5</sup> D. von der Linde, O. F. Schirmer, and H. Kurz, *J. Appl. Phys.* **15**, 153 (1978).

<sup>6</sup> K. L. Sweeney and L. E. Halliburton, *Appl. Phys. Lett.* **43**, 336 (1983).

<sup>7</sup> M. G. Clark, F. J. diSalvo, A. M. Glass, and G. E. Peterson, *J. Chem. Phys.* **59**, 6209 (1973).

<sup>8</sup> F. Agulló-López, G. F. Calvo, and M. Carrascosa, in *Photorefractive Materials and Their Applications*, edited by P. Günter and J. P. Huignard (Springer Verlag, Berlin, in press).

<sup>9</sup> F. Jermann and J. Otten, *J. Opt. Soc. Am. B* **10**, 2085 (1993).

<sup>10</sup> J. Carnicero, O. Caballero, M. Carrascosa, and J. M. Cabrera, *Appl. Phys. B: Lasers Opt.* **79**, 351 (2004).

<sup>11</sup> W. Josch, R. Münser, W. Ruppel, and P. Würfel, *Ferroelectrics* **21**, 623 (1978).

<sup>12</sup> A. Zylbersztejn, *Appl. Phys. Lett.* **29**, 778 (1976).

<sup>13</sup> V. A. Pashkov, N. M. Soloveva, and E. M. Uyukin, *Sov. Phys. Solid State* **21**, 1079 (1979).

<sup>14</sup> J. Feinberg, D. Heiman, A. R. Tanguay, Jr., and R. W. Hellwarth, *J. Appl. Phys.* **51**, 1297 (1980).

<sup>15</sup> B. Sturman, E. Podivilov, and M. Gorkunov, *Phys. Rev. Lett.* **91**, 176602 (2003).

<sup>16</sup> B. Faust, H. Müller, and O. F. Schirmer, *Ferroelectrics* **153**, 297 (1994).

<sup>17</sup> L. Arizmendi, P. D. Townsend, M. Carrascosa, J. Baquedano, and J. M. Cabrera, *J. Phys.: Condens. Matter* **3**, 5399 (1991).

<sup>18</sup> F. M. Michel-Calendini, L. Hafid, G. Godefroy, and P. Moretti,

- Jpn. J. Appl. Phys., Part 1 **24**, 656 (1985).
- <sup>19</sup>L. Hafid, F. M. Michel-Calendini, H. Chermette, and P. Moretti, *Cryst. Lattice Defects Amorphous Mater.* **15**, 97 (1987).
- <sup>20</sup>L. Rebouta, M. F. da Silva, J. C. Soares, M. Hage-Ali, J. P. Stoquert, P. Siffert, J. A. Sanz-García, E. Diéguez, and F. Agulló-López, *Europhys. Lett.* **14**, 557 (1991).
- <sup>21</sup>L. Rebouta, M. F. da Silva, J. C. Soares, J. A. Sanz-García, E. Diéguez, and F. Agulló-López, *Nucl. Instrum. Methods Phys. Res. B* **64**, 189 (1992).
- <sup>22</sup>P. J. Jörgensen, R. W. Bartlett, *J. Phys. Chem. Solids* **30** (12), 2639 (1969).
- <sup>23</sup>N. V. Kukhtarev, *Sov. Tech. Phys. Lett.* **2**, 438 (1976).
- <sup>24</sup>D. Berben, K. Buse, S. Wevering, P. Herth, M. Imlau, and Th. Woike, *J. Appl. Phys.* **87**, 1034 (2000).
- <sup>25</sup>G. de la Paliza, O. Caballero, A. García-Cabañes, M. Carrascosa, and J. M. Cabrera, *Appl. Phys. B: Lasers Opt.* **76**, 555 (2003).
- <sup>26</sup>A. Adibi, K. Buse, and D. Psaltis, *Phys. Rev. A* **63**, 023813 (2001).
- <sup>27</sup>R. S. Weis and T. K. Gaylord, *Appl. Phys. A: Solids Surf.* **37**, 191 (1985).
- <sup>28</sup>P. Herth, D. Schaniel, Th. Woike, T. Granzow, M. Imlau, and E. Krätzig, *Phys. Rev. B* **71**, 125128 (2005).
- <sup>29</sup>G. Martín, G. Rojo, and F. Agulló-López, *J. Appl. Phys.* **95**, 3477 (2004).